

Multi-temporal SAR observations of the Surat Basin in Australia for deformation scenario evaluation associated with man-made interactions

Negin Fouladi Moghaddam¹ · Sergey V. Samsonov² · Christoph Rüdiger¹ · Jeffrey P. Walker¹ · Walter D. M. Hall³

Received: 9 April 2015 / Accepted: 25 July 2015 / Published online: 9 February 2016
© Springer-Verlag Berlin Heidelberg 2016

Abstract Human activities for extracting natural resources, may lead to subsequent gradual or abrupt surface deformation, with adverse effects in the local ecosystem and damage to man-made structures. Over the past two decades, interferometric SAR (InSAR) has been demonstrated as the optimal remote sensing technique to estimate surface deformation with high spatial coverage and vertical accuracy over traditional surveying methods. In this paper, the outcome of advanced differential InSAR processing to detect and analyze ground surface behavior due to man-made interactions are presented. An improvement was achieved in the temporal resolution and accuracy using a unique combination of both C-band and L-band SAR satellite acquisitions with different temporal and spatial baselines. The two alternate DInSAR methodologies were applied on the northeastern part of the Surat Basin, Australia for an area without long-term ground-based geodetic observations. The regions undergoing downward motion are located above coal seam gas (CSG) mining sites with rates up to 28 mm/year. Three scenarios were identified: (1) extensive groundwater extraction from shallow aquifers due to CSG mining, (2) CSG mining without direct impact on groundwater resources and (3) patchy uplift over an industrial forest adjacent to a CSG mining district.

Contrary to a previous study conducted in this region using the PSInSARTM technique which reported stability of the area with insignificant surface deformation, this study shows that there are considerable deformation signals consistent with resource extraction. Consequently, it is shown that the SBAS approach is superior to PSInSARTM for deformation monitoring with focusing on naturally distributed scatterers.

Keywords Surface deformation · InSAR · SBAS · Time series analysis · Surat Basin · Australia

Introduction

Coal bed methane (CBM) is the methane gas captured and released from coal seams around the world, with the highest production in China and the US, followed by Russia, Australia, Ukraine and India. This underground resource has drawn attention for being both a greenhouse gas (GHG) and an environmentally friendly fuel compared to conventional gas resources (Karacan et al. 2011).

Over the past decade, the CBM industry in Australia has experienced substantial growth by commercial production of coal seams in a vast extent of the Surat and Bowen Basins in southern Queensland. These basins contain 95 % of the known Australian reserves. The targeted shallow (i.e., 200–600 m below surface), low-rank coal layers with high permeability have justified low cost and viable extraction of CBM over the past years, to meet growing domestic and international demands for energy supply (Papendick et al. 2011; Hamilton et al. 2012).

Underground coal seams extending through impermeable geological layers hold natural gas, mostly dominated by biogenic methane. Under natural conditions this gas,

✉ Negin Fouladi Moghaddam
negin.moghaddam@monash.edu

¹ Department of Civil Engineering, 23 College Walk, Monash University, Clayton, VIC 3800, Australia

² Canada Centre for Mapping and Earth Observation, Natural Resources Canada, 560 Rochester Street, Ottawa, ON K1A0E4, Canada

³ School of Earth, Atmosphere and Environment, Monash University, Clayton, VIC 3800, Australia

which is attached to the coal layers and held in place by hydrostatic pressure of the water in the coal beds, can be extracted simultaneously by removing some of the formation water and drawing the reservoir pressure down to a level that allows the gas to desorb. In other words, CBM production does not dewater the aquifers but only extracts 200 GL/year estimated peak of saline water from the coal formations, to depressurize the coal seams (DNRM 2012). Approximately 35–40 m drop in the water level above the gas producing coal seams will result in the essential rate of depressurization for gas production. The volume of produced water, which is relatively high compared to the volume of gas in the early stages of production, is subsequently reinjected into an underground formation or is discharged to the surface (Veil et al. 2004; CSIRO 2012). The rate of water withdrawal from coal layers is about 18,000 ML/year, which is far greater than that during conventional hydrocarbon production (APLNG 2010; QWC 2012). Consequently, hydrogeological assessment has indicated that long-term CSG mining and accompanied groundwater extraction put a number of fresh water storages under progressive depletion and head decline (Tan et al. 2010). Potential changes in pressure and stress conditions within the sub-surface and surrounding geology, induced by these anthropogenic activities, can be projected onto the surface as deformation after considerable compaction or expansion of the sub-surface reservoir (Galloway et al. 1998; Dzurisin 2007).

Ground surface deformation resulting from oil and gas production and geothermal activities (Fielding et al. 1998; Burgmann et al. 2000), groundwater extraction (Massonnet and Feigl 1998; Chaussard et al. 2014) and mining developments (Fialko et al. 2002; Deguchi et al. 2007; Samsonov et al. 2013) can be used to better identify the geomechanical and geological properties of a reservoir, and to mitigate the operation risk throughout the CO₂ storage procedure (Vasco et al. 2010). Consequently, a number of monitoring techniques to measure surface (tilt meter, leveling, GPS, InSAR) and sub-surface (extensometer, 4D seismic surveys) changes have emerged to detect the extent of the deformation and to quantify the rate of the deformation over extraction or injection sites. Some of these techniques have limited and sparse data sampling (i.e., seismic lines or boreholes) while others fail to map geological properties directly (Brown et al. 2014). However, among the various geodetic measurement tools, InSAR (a remote sensing tool) can not only be used to constrain the geophysical parameters of the reservoir (Sambridge 1999), but its cost-effective and high temporal resolution data acquisition can also complement other traditional measurements such as GPS (Zhu et al. 2014) and sub-surface images captured by seismic surveys (Ramirez and Foxall 2014). Moreover, compared to geophysical surveys, InSAR

observations have demonstrated the potential for mapping the underlying sub-surface structure by detecting long-term deformation patterns on the surface due to changes in sub-surface volume and pressure (Anderssohn et al. 2009; Vasco et al. 2010). These studies suggest that the deformation patterns might also be an indication for the sub-surface structural properties which are usually captured for the rock mass by geophysical measurements (Amelung et al. 1999; Hatherly 2013).

Measuring ground displacement using satellite SAR interferometry and its integration with GPS survey data have been performed in Australia for underground mining operations (Ng et al. 2012; Zahiri 2012; Featherstone et al. 2012) and for earthquake risk assessment (Dowson et al. 2008). But for the Surat Basin, the CSG authorities initiated a ground motion baseline program. Their objective was to report any high motion with reference to natural or anthropogenic characteristics (QGC 2013). From their analysis, advanced InSAR technology—PSInSARTM (Ferretti et al. 2001) with about 600 permanent scatterers per km²—did not show any large-scale pattern of ground motion between 2006 and 2011, thus reporting to be in the stable condition with less than 8 mm ground deformation per year (Dura et al. 2012). For the same area, Geoscience Australia conducted an independent study to describe the capabilities and limitations of an analytical model to predict surface deformations caused by fluid volume changes. Based on their analysis, maximum potential for surface deformation was predicted to be less than 0.2 m. Assuming that the regional drawdown is around 300 m. InSAR observations were suggested to be examined as a valuable tool to constrain the parameter space, and to develop a surface deformation prediction (Brown et al. 2014).

Taking into account the previous studies, this paper presents an interferometric analysis across the same region within the Surat Basin (Fig. 1), for which surface deformation of an area between Miles and Dalby was reported through in situ observations (DNRM 2012). These field surveys, which contradict previous InSAR results, were considered as the starting point for verifying results using this new multi-temporal and high-resolution SAR analysis from C-band (ERS1/2, ENVISAT and RADARSAT-2) and L-band (ALOS PALSAR) microwave sensors, together with an alternative processing approach.

Geological context

The Surat Basin is an intracratonic geological basin complex with an area of 270,000 km² within northeastern Australia (Fig. 1) that overlies parts of the Bowen Basin. Sedimentation in this basin commenced from the Early Jurassic, while by the Middle Jurassic swamp

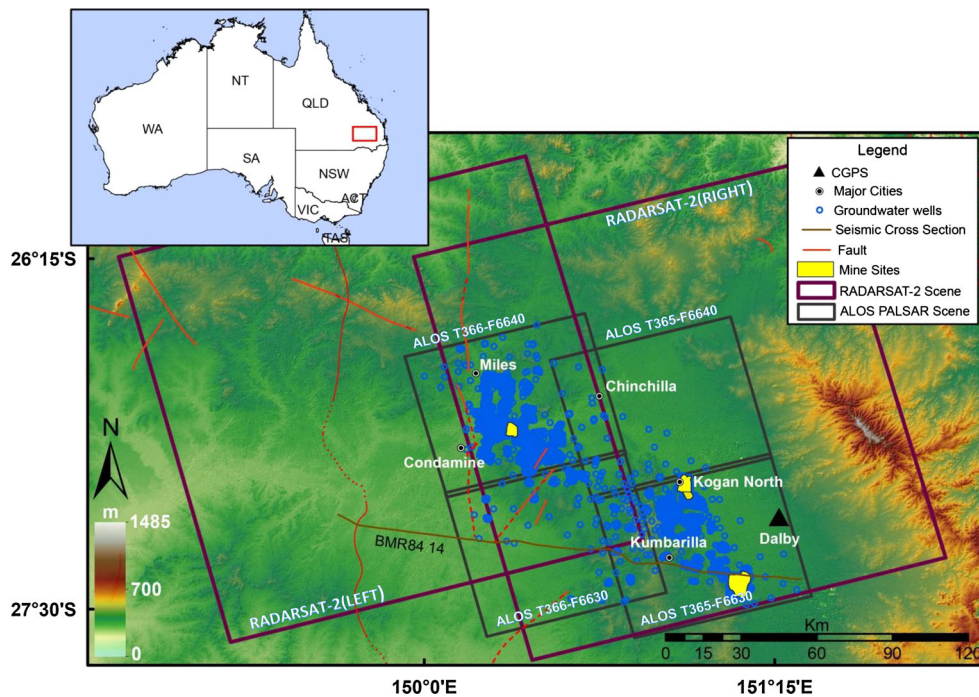


Fig. 1 Location map of the study area in the Surat Basin showing C-band (RADARSAT-2) and L-band (ALOS PALSAR) satellite footprints in image mode over the 90 m SRTM digital elevation model. Four scenes of ALOS PALSAR (gray squares) and two scenes of RADARSAT-2 (purple squares), both in ascending paths, cover the region of interest for 2006–2011 and 2012–2014, respectively.

Clusters of groundwater extraction wells shown with *blue dots* are associated with CSG mining districts in *yellow polygons*. The fault traces are shown in *red*. The *triangle* marks the location of a continuous GPS station. To demonstrate the sub-surface image of this part of the Surat Basin, BMR84-14 seismic line (in *brown color*) is shown in Fig. 2

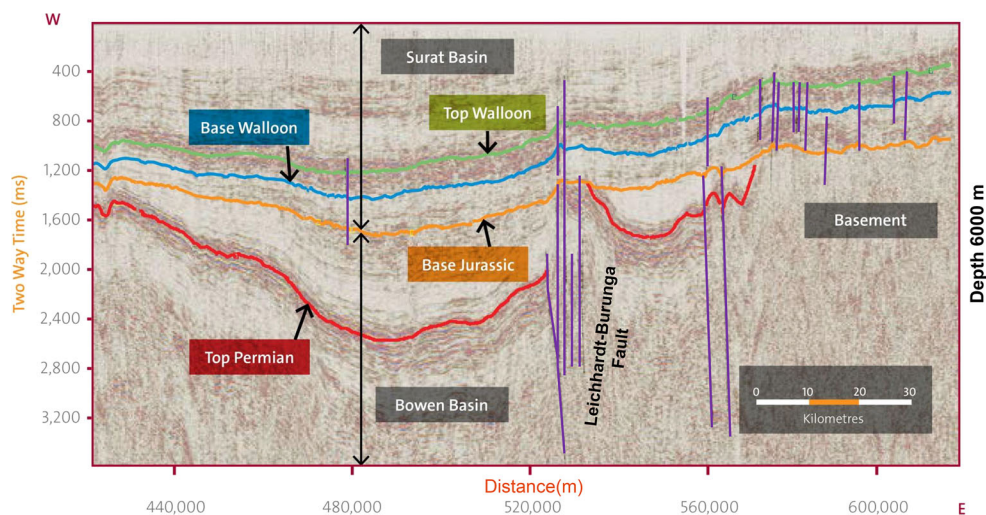


Fig. 2 Normal-polarity seismic section (BMR84-14) which passes across the southern part of the Surat Basin (Fig. 1) shows a sequence of sedimentary rocks. Seismic reflections at each lithological boundary (i.e., seismic reflectors) result from changes in acoustic impedance (AI) of the traveling seismic wave. AI represents the predictable and characteristic acoustic properties of a rock and is the product of rock density and seismic velocity. To investigate rock units in the sub-surface, there should be a significant AI contrast (Badley

1985). The Bowen Basin lies below the *yellow horizon*, while the Surat Basin overlies it (shown with *vertical black arrows*). The *colored lines* show the top of each sub-surface formation in seismic two way time (TWT). WCM are shown by the bright reflections limited by the *green and blue seismic markers*. Sudden change in the formation type could be an indicator for fault locations (e.g., Leichhardt–Burunga Fault) (after Martin et al. 2013; QGC 2013)

environments predominated over much of the basin, with minor erosional unconformities (Exon 1976; Scott 2008). Sediment accumulation in the Surat Basin was terminated in mid-Cretaceous times. Minor extensional fault movements characterized the Paleocene period, associated with the opening of the Coral Sea, and mild compressive deformation in Oligocene–Miocene times coincided with a major phase of basaltic volcanism in eastern Australia. In the Tertiary and Quaternary times, the area evolved through erosion to its present topographic relief (Fielding et al. 1996; Cadman and Pain 1998). The structural framework of this part of the basin is controlled by the Burunga–Leichhardt thrust fault system which remained active throughout deposition of the Surat Basin succession, controlling its depositional architecture (Hamilton et al. 2012).

As part of the Great Artesian Basin (GAB) (Green et al. 1997), one of the world's largest underground water resources, the Surat basin comprises different geological layers (Fig. 2). Some of the layers are porous aquifers which are accessed by water bores for farming and groundwater supply. Below the main aquifers, denser and less permeable the Walloon Coal Measures (WCM) hosts the target coal seam in the Surat Basin which separates two major aquifers, the Hutton Sandstone (Early–middle Jurassic) and the Springbok Sandstone (Late Jurassic). Fractured coal seam aquifers are considered as one of the major sources of groundwater (Hamilton et al. 2012). The reported depressurization in groundwater aquifers and associated leakages have the potential to reduce groundwater supplies in the GAB aquifer, to limit natural groundwater discharge, and to cause compaction of geological layers which may result in subsidence on the surface (QWC 2012).

Methodology

Interferometric analysis

Recent advances in synthetic aperture radar (SAR) remote sensing technologies and in processing techniques now make it possible to map large-scale deformation patterns with amplitudes on the order of a few centimeters. Over the past decade, interferometric SAR has been demonstrated as the optimal remote sensing technique to estimate ground surface deformation induced by over-exploitation of underground resources (Lanari et al. 2004; Galloway and Hoffman 2007; Chaussard et al. 2013); however, the growing number of satellite data sources and advanced processing techniques make this technology as a standard and widespread tool for reservoir management and risk assessment (Ferretti 2014).

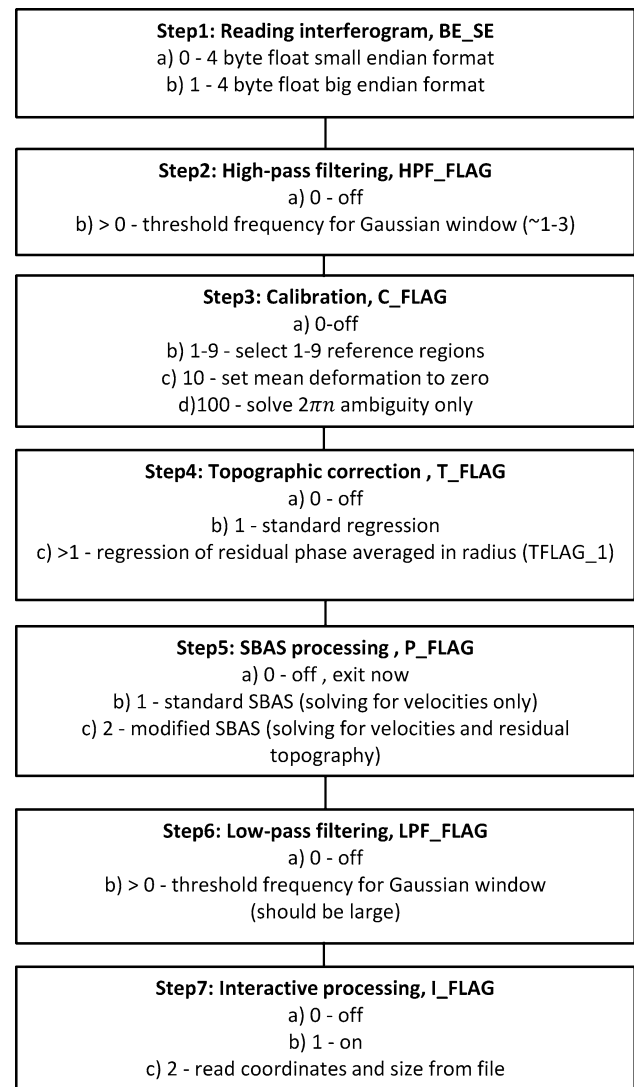


Fig. 3 Flowchart diagram of the code used for time series calculation and mean/linear deformation rate estimation in both ALOS PALSAR and RADARSAT-2 satellite observations. Flags (_FLAG) specified in a header file are used for controlling processing flow (Samsonov et al. 2011)

Synthetic aperture radar (SAR) is a technology that measures the return of an actively emitted microwave signal from a target. Due to the nature of microwave energy as an illuminating source in radar sensors, this technology does not rely on solar irradiation, making it more versatile than traditional passive sensor technologies. More importantly, it suffers only limited disturbance from atmospheric conditions, meaning that it has an all-weather observing capability. Imaging radar sensors emit signals in a specific portion of the chosen electromagnetic spectrum, which is generally based on their operational purpose. The near-polar orbit of these satellites, in combination with the Earth's east–west rotation, theoretically allow observing the same area from two different look

Table 1 SAR data used for DInSAR processing in this work: time span (in YYYYMMDD format), azimuth θ and incidence angles ϕ , number of available SAR images N and number of calculated interferograms M

InSAR set	Time span	Resolution (m)	θ ($^\circ$)	ϕ ($^\circ$)	N	M
ERS1, track 216 (dsc)	19920725–19930116	7.9–4	–164.45	23	3	3
ERS2, track 216 (dsc)	19951121–19951226	7.9–4	–164.45	23	2	1
ERS1, track 488 (dsc)	19920604–19950826	7.9–4	–164.45	23	5	5
ERS2, track 488 (dsc)	19960114–19991025	7.9–4	–164.45	23	2	1
ENVISAT, track 216 (dsc)	20031209–20051108	7.8–4	–164.50	23	6	5
ENVISAT, track 488 (dsc)	20040725–20060101	7.8–4	–164.50	23	5	4
ALOS, track 365, frame 6630 (asc)	20070103–20110301	4.7–3	–14.66	39	20	37
ALOS, track 365, frame 6640 (asc)	20070103–20110301	4.7–3	–14.58	39	20	38
ALOS, track 366, frame 6630 (asc)	20061205–20110131	4.7–3	–14.66	39	22	60
ALOS, track 366, frame 6640 (asc)	20061205–20110131	4.7–3	–14.58	39	22	61
RADARSAT-2, right (asc)	20120703–20140530	12.5–12.5	345.44	35.6	22	75
RADARSAT-2, left (asc)	20120720–20140429	12.5–12.5	345.44	35.6	21	134
Total					150	424

angles on each satellite orbit, i.e., ascending and descending with different incidence angles. Combining these observations not only mitigates the problems arising due to acquisition geometry and uneven sampling on hilly terrain areas, but can also distinguish between vertical and east–west motions (Ferretti et al. 2007; Simons and Rosen 2007).

The main principle in SAR interferometry is to compare the phase of two or more radar images which are typically acquired from the same flight track but at different times. This technique, which is known as differential InSAR, is used to determine displacements of the Earth’s surface at wavelength scale. SAR satellites observe the ground in a non-vertical LOS direction. In zero-baseline condition, the phase information would only be related to the LOS displacement while in reality a certain baseline is always present making the interferogram sensitive to the topography. By using an external digital elevation model (DEM), the topographic phase contribution will be subtracted from the interferogram, leading to a differential SAR interferogram that can be used to detect subtle changes (e.g., deformation) in the range distance between two acquisitions (Goldstein 1995; Zebker et al. 1997).

Stacking method for interferometric analysis

To calculate the ground deformation phase captured by SAR technology, other phase components including orbital ramps, atmospheric artifacts, topographic residuals and thermal dilations should be removed or mitigated. Considering the fact that differential interferograms have been successfully unwrapped, orbital ramps corrected, and

regions with coherence below the threshold are set to zero, each k interferogram ϕ_{obs}^k is the sum of deformation ϕ_{def}^k residual topographic ϕ_{topo}^k , and atmospheric ϕ_{atm}^k components:

$$\phi_{obs}^k = \phi_{def}^k + \phi_{topo}^k + \phi_{atm}^k \tag{1}$$

The goal is, therefore, to estimate and remove the residual topographic ϕ_{topo}^k and atmospheric ϕ_{atm}^k components to achieve the best possible accuracy in the calculation of the ground deformation ϕ_{def}^k . For simplification of the atmospheric noise contribution, it is assumed that ϕ_{atm}^k contains all other random noise sources such as atmospheric temperature and water vapor (Tarayre and Massonnet 1996).

For processing SAR images with the DInSAR technique, a simulated elevation model is used to remove the main topographic phase contribution, but the outcome is still prone to temporal and spatial decorrelation, which impacts on the number of useful differential pairs and imposes a phase unwrapping deficiency in rough areas or for complicated ground movements (Gabriel et al. 1989; Zebker and Villasenor 1992). It is also possible that particular patterns of subsidence make it difficult to separate between deformation signals and atmospheric artifacts, and this has led to the development of a technique called stacking which is based on a set of interferograms covering the same area within a given time period, reducing the ratio between atmospheric effects and deformation signals (Sandwell and Price 1998; Petrat and Wegmuller 2003). When stacking interferograms, the weighted average of all the deformation velocities within the single interferogram is used to estimate the mean deformation rate for each

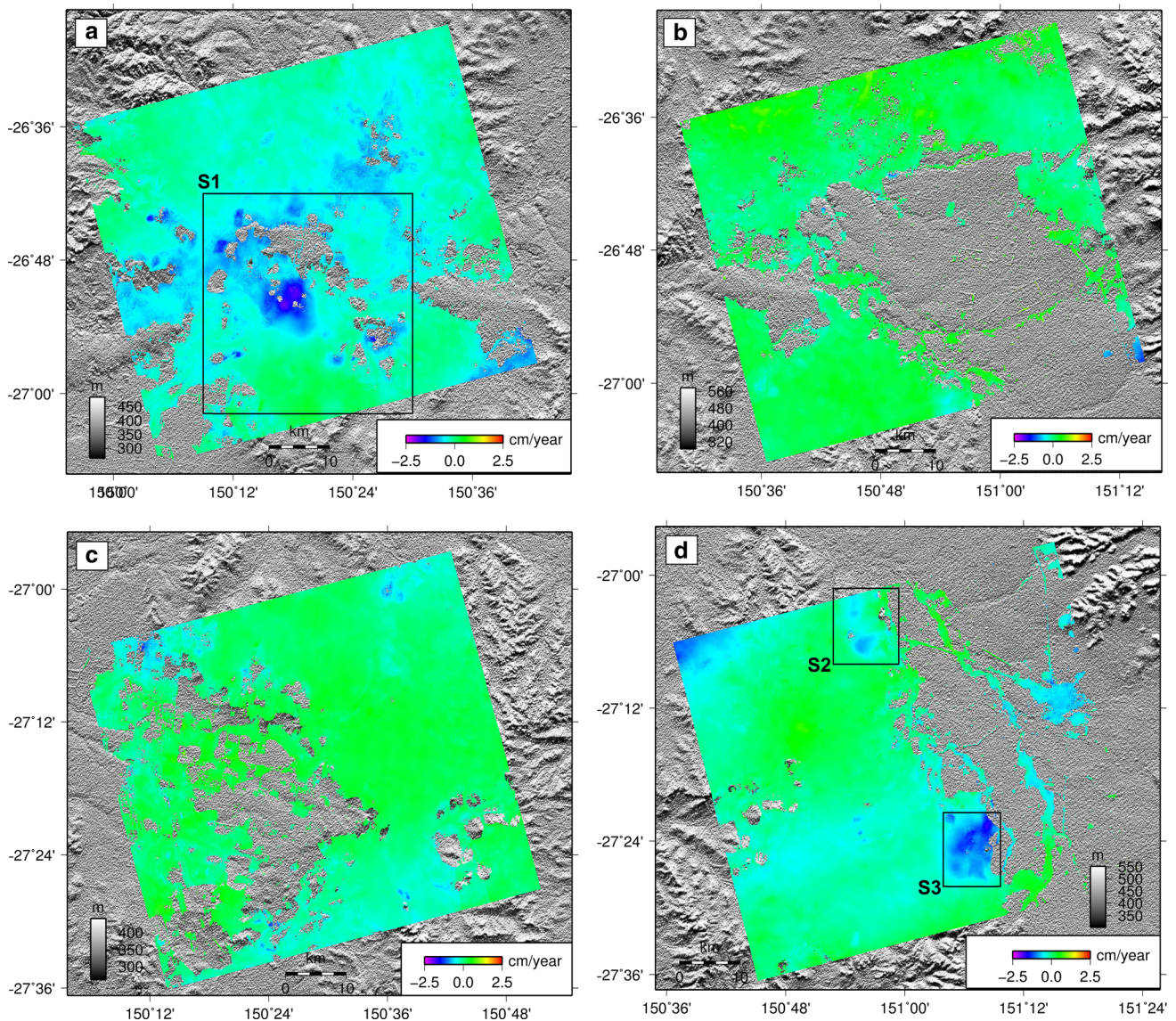


Fig. 4 Line of sight deformation rates (in cm/year) from stacking of ALOS PALSAR ascending scenes: **a** T366-F6640; **b** T365-F6640; **c** T366-F6630; **d** T365-F6630 between 2006 and 2011. Based on the processing results, among four ALOS scenes, significant phase delay

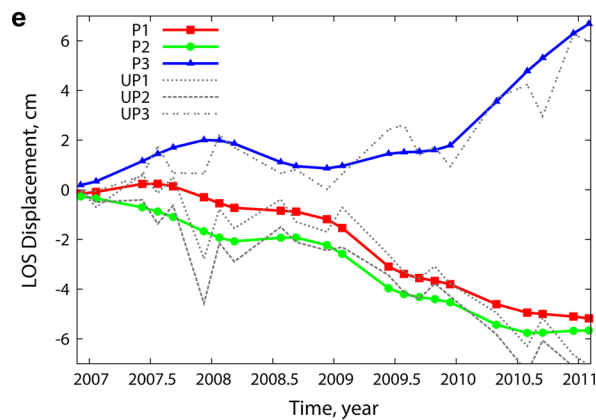
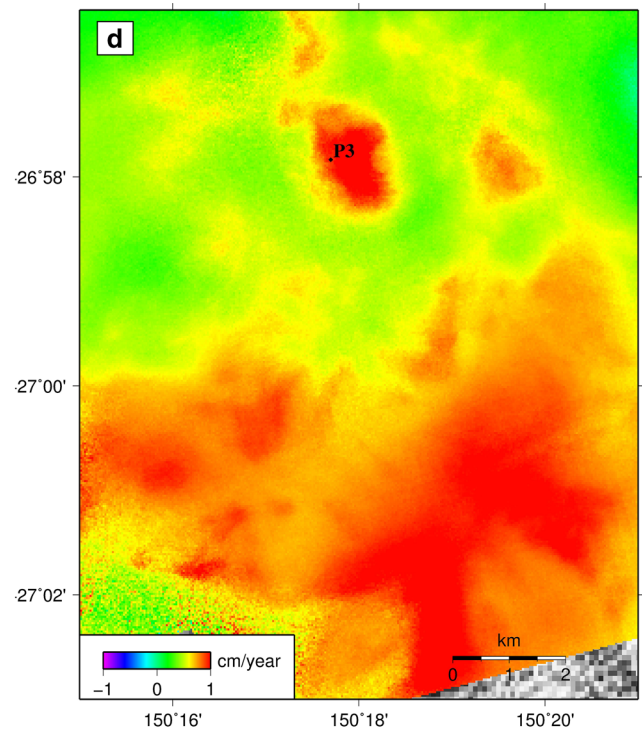
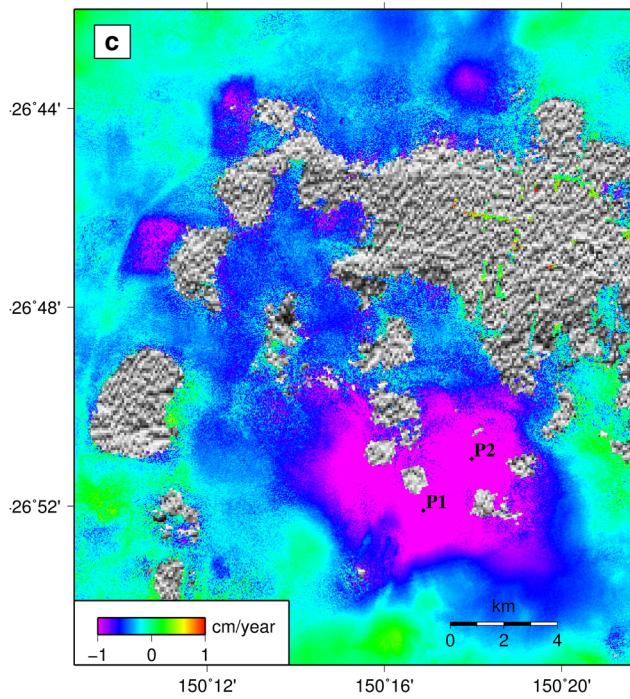
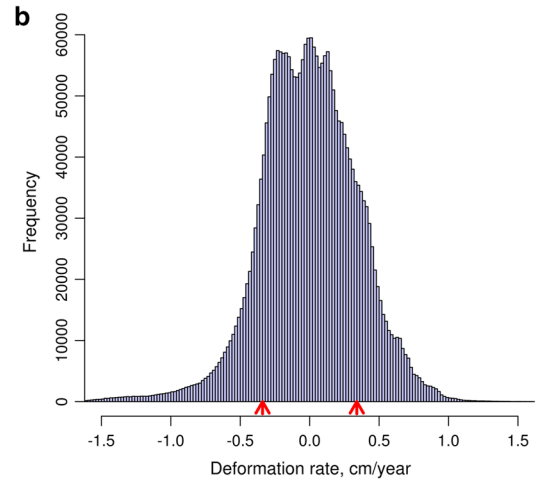
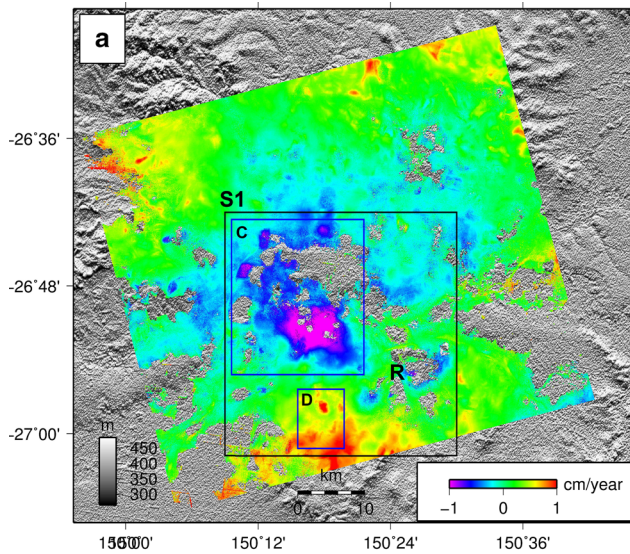
pixel. These weights are selected based on the corresponding time spans (Sansosti et al. 2010).

As long as the images are sufficiently separated in time, the phase noise in a stacked interferogram will be a factor of \sqrt{K} , where K is the number of interferograms and noise will reduce to approximately $1/\sqrt{K}$. In this case, the averaged interferogram is less noisy than any of the original interferograms but with reduced amplitude. Stacking is the best processing solution when scarcity in the number of satellite observations prevents the application of advanced techniques, similar to the situation in the Surat Basin for ESA archived C-band satellite observations (Moghaddam et al. 2013). It is also an acceptable approach if the noise is

responses were detected in **a** and **d**; however, the other two scenes show no signal of ground movement. Locations S1, S2, and S3 are candidate sites with downward motion, closely aligned to the areas with CSG mining

Fig. 5 SBAS analysis results for T366-F6640 with 22 ALOS PALSAR FBS-FBD imagery. **a** The rate of deformation (cm/year) in LOS direction. **b** The frequency distribution of deformation rate for the best reference point (R in **a**) after implementing Gaussian filtering in time domain. **c, d** Selected points ($P1, P2, P3$) for time series analysis over the areas with downward and adjacent upward motion in candidate region $S1$. **e** Time series of ground surface deformation for selected points relative to the assigned reference in LOS direction before Gaussian filtering (UP_x) and after filtering (P_x)

random and normally distributed. When stacking fails to be an effective technique because the noise in the interferograms is not normally distributed, more advanced processing techniques are required (Zebker et al. 1997; Williams et al. 1998).



Small baseline subset (SBAS) for interferometric analysis

Conversely to stacking, small baseline subset (SBAS) (Berardino et al. 2002; Casu et al. 2008) as an evolution of DInSAR techniques uses a cluster of SAR acquisitions to create a back-scattering time series. This method has proven to be the most accurate for mapping various sources of ground deformation, including seismic and volcanic displacements, subsidence due to fluid extraction, and many other natural and anthropogenic phenomena (Samsonov and D'Oreye 2012).

SBAS was developed to create time series of deformation with reduced atmospheric, orbital and thermal signals by increasing the number of ground points, and by reducing the baseline length for each of the data pairs (Samsonov et al. 2011; Hooper et al. 2012). After ensuring that the image network has no isolated image cluster (fewer than five images) the interferograms are formed. The critical step in this algorithm is the identification of potentially coherent points using image pairs with estimated correlation above a threshold value (based on the expected rate of decorrelation and data availability for a given region). Moreover, it improves the coherence by producing a large number of small baseline multi-reference interferograms using a single value decomposition (SVD) algorithm by building an optimal set of interferograms having the smallest temporal and baseline decorrelation, and using several master images (Berardino et al. 2002).

This technique makes it possible to perform time series analysis and to extract the linear deformation rates from a set of co-registered, unwrapped differential interferograms using a linear least squares inversion. The flowchart in Fig. 3 presents the processing stages which were completed in this study for L-band and C-band satellite observations with high acquisition frequency over the proposed area. Calculating deformation rates, reconstruction of cumulative displacements (time series), and estimating mean and linear deformation rates are the tasks performed by this methodology (Samsonov et al. 2011).

Data processing

Assuming that there is no prior information about the exact location of deformation in this part of the Surat Basin, an initial monitoring of the area with large spatial satellite datasets was undertaken to identify potential areas of subsidence or uplift due to underground resource extraction. Performing a standard DInSAR processing for ENVISAT ASAR image mode in four descending tracks and an average revisit frequency of 35 days revealed that two scenes covering the area between Miles and Dalby

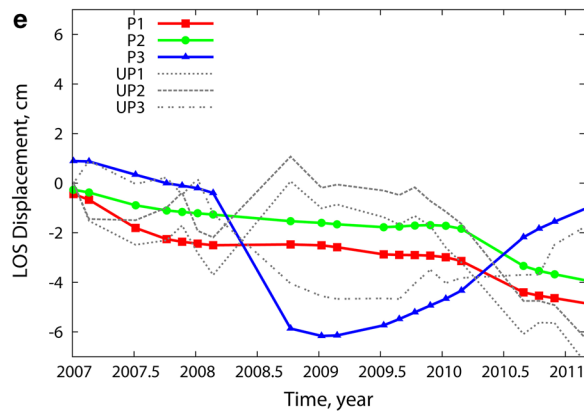
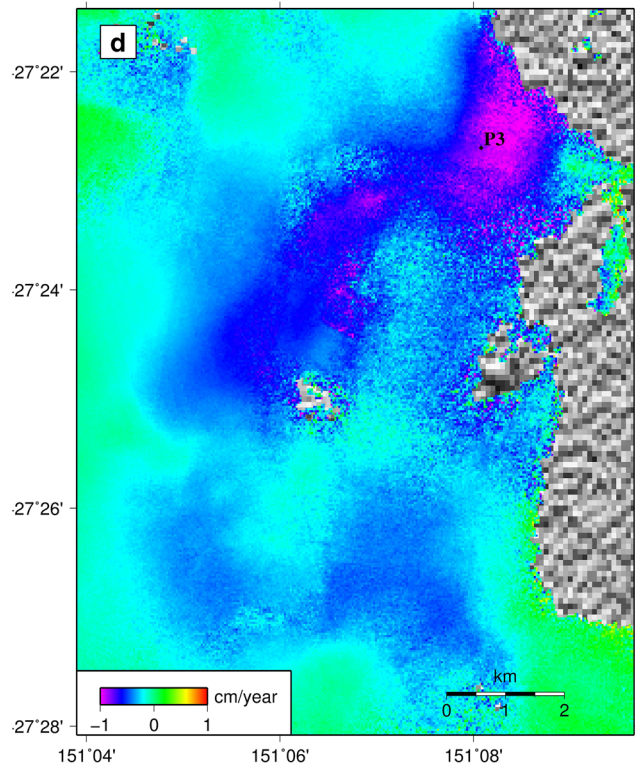
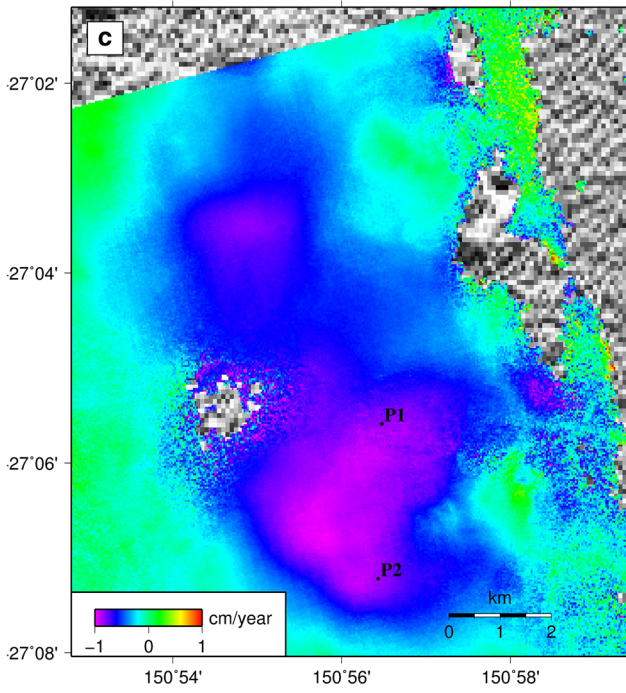
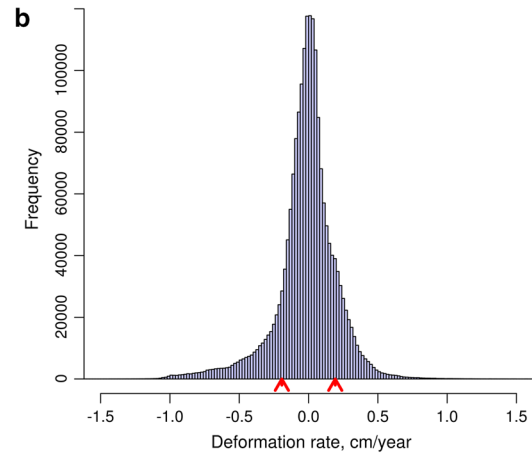
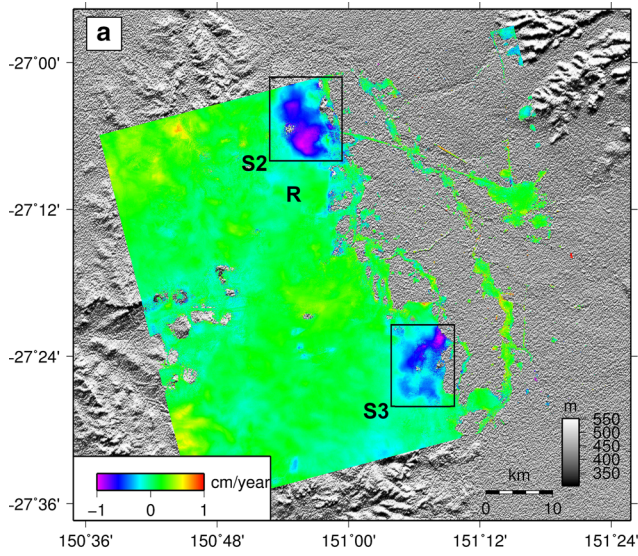
Fig. 6 SBAS analysis results for T365-F6630 with 20 ALOS PALSAR FBS-FBD imagery. **a** The rate of deformation (cm/year) in LOS direction. **b** The frequency distribution of deformation rate for the best reference point (R in **a**) after implementing Gaussian filtering in time domain. **c, d** Selected points ($P1, P2, P3$) for time series analysis over the areas with downward motion in candidate regions $S2$ and $S3$. **e** Time series of ground surface deformation for selected points relative to the assigned reference in LOS direction before Gaussian filtering (UP_x) and after filtering (P_x)

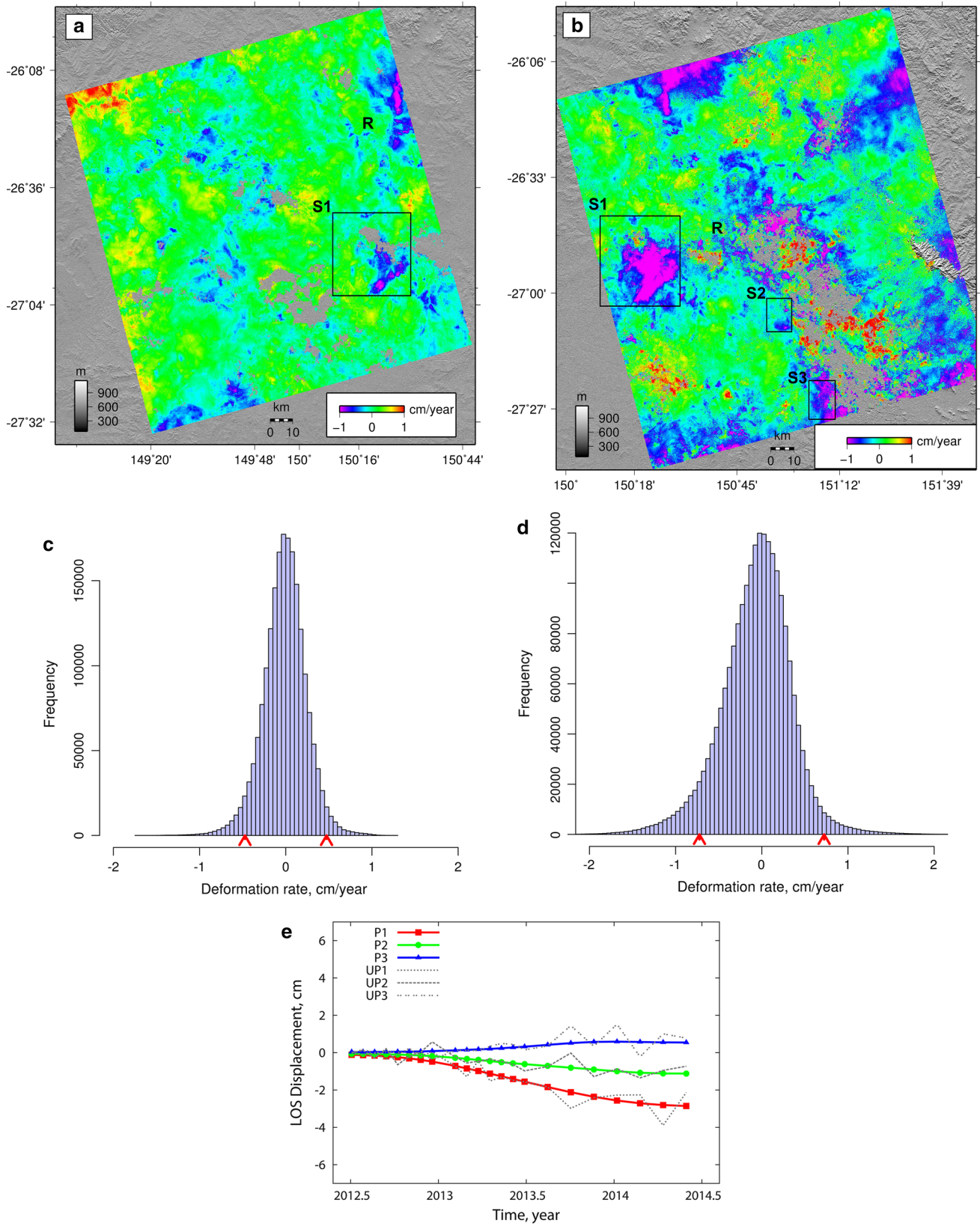
have captured what appears to be surface deformation, due to consistency in the signal's phase delay during the time of observation (Moghaddam et al. 2013). Accordingly, the focus of further analysis was on the processing of more high-resolution satellite imagery covering the same area with a higher temporal and spatial resolution.

To screen the long-term behavior of the ground surface and to estimate the rate of deformation in the focal area of the Surat Basin, a standard DInSAR processing including orbit correction, phase unwrapping and geocoding for both C- and L-band SAR images (Table 1) with temporal and spatial baseline smaller than the predefined threshold values was performed. This was followed by the stacking technique for interferograms with high coherence and low unwrapping errors, to remove residual orbital ramps and long wavelength atmospheric noise.

In the case of ERS1/2 (1992–1999) and ENVISAT (2003–2006), the scarcity of data coverage and the low number of interferograms prevented coherent results being achieved using stacking, though the stacking stage was successful for the ALOS PALSAR (2006–2011) dataset. Checking the Japan Aerospace Exploration Agency (JAXA) archive for ALOS PALSAR indicated that four L-band scenes (T365-F6630, T365-F6640, T366-F6630 and T366-F6640) with approximately 20 images per scene cover the focus areas (Fig. 1). Applying the stacking algorithm over this dataset and at the same time having a sufficient number of interferograms ultimately provided a better cumulative phase delay response with less noise contribution. Stacking results for each scene suggested that among the four ALOS PALSAR scenes, both T365-6630 and T366-6640 have significant deformation signal patterns after 2007 (Fig. 4a, d).

Based on the initial processing results using stacking and predetermined deformation signals in the region, the SBAS code (Samsonov et al. 2011), which functions as an advanced InSAR processing technique to solve for deformation rate and the residual topographic noise simultaneously, was applied for both ALOS PALSAR archived images and RADARSAT-2 new acquisitions (Table 1). The analysis of ALOS PALSAR observations is from 05 December 2006 through 31 January 2011 and includes different acquisition time frequencies for single (FBS) and for dual beam (FBD) modes. To apply the SBAS approach,





◀ **Fig. 7** SBAS analysis results for RADARSAT-2. **a, b** The rate of deformation (cm/year) in LOS direction for RADARSAT-2 *left* and *right* in Fig. 1, respectively. **c, d** The frequency distribution of deformation rate for the best reference points (*R* in **a, b**) after implementing Gaussian filtering in time domain. **e** Graph illustrates the time series of ground surface deformation for selected points relative to the assigned reference for RADARSAT-2 *right*

a parameter file consisting of all interferograms with high coherency, i.e., more than 0.3, was required. The most coherent interferograms for this purpose were selected through calculating the mean coherence of each interferogram. Using such an approach, the linear rate of deformation for both scenes (Figs. 5a, 6a) and its corresponding error were generated.

To estimate the accuracy of the deformation measurement, LOS linear deformation rates resulting from SBAS for each of the two datasets (assuming here T366-F6640 and T365-F6630 as one set each) were plotted for four different reference points. These points were selected in regions with good coherence (Figs. 5a, 6a; *R* in green areas on the maps). To test the hypothesis of these points being suitable reference points, the frequency distribution (histogram) of each relative linear deformation rate was plotted and its statistics estimated (i.e., mean, mode and standard deviation) on a cm/year scale. Based on the estimated mode (i.e., the most frequent value of deformation rate in cm/year or stable areas), the values corresponding to the motion greater than the mode of the distribution were selected and the remaining values removed. To produce a Gaussian distribution, the mirrored values of those for which standard deviation (σ) was estimated ($\sigma = 0.34$ cm/year for T366-F6640 and $\sigma = 0.21$ cm/year for T365-F6630) were then added. In this case, the absolute values corresponding to the motion greater than 2σ cm/year representing true ground deformation with probability 95 % were estimated (Casu et al. 2006; Samsonov et al. 2014). Practically, for T366-F6640 (Fig. 5b), it could be claimed that true subsidence in LOS was less than -0.68 cm/year while for T365-F6630 (Fig. 6b), it could be claimed that deformation values change between ± 0.42 cm/year.

Initial time series reconstruction of the linear deformation rates for both scenes has shown seasonal patterns [i.e., gray lines for UP_x ($x = 1, 2, 3$) in both Figs. 5e, 6e] which should be mitigated to extract important statistical properties of a time series including its direction (trend) and its turning. Seasonal pattern can conceal these features by making period-to-period movements in the data (Statistics Canada 2009). For this purpose, and to extract smoothed cumulative displacements, Gaussian filtering as a separable and low-pass filter was implemented to adjust each observation epoch in the temporal domain. To remove the high-frequency component, the shape of the filter was defined as a function of standard deviation in seconds.

Smoothing with good localization then resulted from using a Gaussian filter with 3σ window size in each direction making it possible to interpret the ground surface deformation signals and to extract the trend in the selected points (i.e., colorful lines for both Figs. 5e, 6e).

Time series analysis of T366-F6640 (Fig. 5e) demonstrates that in S1 region, both P1 and P2 experienced downward motion since 2007 while P3 showed an uplift behavior. Moreover, the rate of deformation in P1 was slightly larger than that in P2. Both P1 and P2 are located over a coal seam gas mining area called Berwyndale South, close to Condamine (Fig. 1) while P3, which appeared with an upheaval signal, is in the vicinity of an industrial timber forest. The reason for the upward motion is not injection in this part of region S1, but the shallow depth formations with elasto-plastic properties. The situation brings that P3 went up to respond to the adjacent gradual downward motion in areas with subsidence signals.

For T365-F6630 (Fig. 6e), all selected locations in S2 and S3 regions, which are CSG mining districts, display a downward motion since 2007. But their temporal patterns are not similar; while P1 and P2 shift downward gradually, with higher rate for P1, P3 seems to sink abruptly after 2008. However, by the start of 2009, P3 commenced to recover with an ongoing uplifting. Although the two regions enclosed CSG operation areas, the geological conditions and depth of mining are different in each of these areas.

It is worth mentioning that when the proposed area was monitored by recent RADARSAT-2 acquisitions during 2012–2014 (Fig. 1) using the same processing approach, the results were comparable to the ALOS PALSAR observations. As shown in Fig. 7a, b, the previously mentioned regions S1, S2, and S3 have still retained their gradual settlement to the present day. Due to the swath of the satellite scene, RADARSAT-2 (left) image did not cover the S2 and S3 regions, but they are covered in the RADARSAT-2 (right) image. Figure 7c, d depicts the frequency distributions of the scenes for the selected reference point (*R*) after applying Gaussian filtering. Graph 7e represents the ground surface behavior in RADARSAT-2 (right)-S1 region for three previously mentioned points before and after Gaussian filtering. For the observation time which was covered by RADARSAT-2 (2012–2014), the ground surface retained its deformation pattern. In other words, P1 and P2 were still experiencing downward motion, while P3 kept shifting upward to present day.

Results and discussion

To complement recent field studies conducted in the northeastern part of the Surat Basin (QWC 2012) a cost-efficient remote sensing tool with a large spatial extent and

Table 2 Correlation coefficient estimation for each resource extraction site with displacement

Daandine	Deformation	Coal seam gas	Groundwater
Displacement	1	-0.92	-0.46
Coal seam gas	-0.92	1	0.63
Groundwater	-0.46	0.63	1
Tipton West Groundwater	Deformation	Coal seam gas	
Displacement	1	-0.84	-0.89
Coal seam gas	-0.84	1	
Groundwater	-0.89	0.86	1
Berwyndale South Groundwater	Deformation	Coal seam gas	
Displacement	1	-0.76	0.86
Coal seam gas	-0.76	1	-0.48
Groundwater	0.86	-0.48	1
Kogan North Groundwater	Deformation	Coal seam gas	
Displacement	1	-0.86	0.88
Coal seam gas	-0.86	1	-0.81
Groundwater	0.88	-0.81	1

high temporal resolution has been used. In-depth analysis of the InSAR deformation maps for three candidate regions (S1, S2, S3) shows substantial ground settlement sites located in the vicinity of extraction areas. To interpret these results for further studies including sub-surface modeling, the integrity of the mapped deformation signals needs to be verified. As discussed above, most regions have undergone gradual ground settlement since 2007 with increasing downward motion toward 2014. However, the rate of settlement has decreased and even reversed during the period 2008–2009.

Given that levelling or three-dimensional high-frequency measurements of ground motion by a global positioning system (GPS) receiver installed at a subsiding site can map the progress of subsidence as a function of time (Hofmann-Wellenhof et al. 2001) and can act as an independent geodetic method to verify the interferometric results (Casu et al. 2006), the availability of continuous geodetic data within the region for our specific observation time (2006–2014) has been checked. The only available GPS time series is from a station located in Dalby (Fig. 1) between June 2010 and June 2014. However, this station is not useful in this case as the deformation detected from the space-borne sensors occurred farther away and is localized. Therefore, the available data on CSG and ground water extraction rate were checked for matching patterns in the surface deformation development.

For the three regions previously identified by InSAR measurements as undergoing deformation spots, the correlation coefficients were calculated to quantify the strength and direction of the relationship between groundwater and CSG extraction, CSG extraction and displacement, and groundwater extraction and displacement (see Table 2).

According to Fig. 8a, b accompanied with Table 2, displacement rate per year is highly correlated with CSG extraction. Significant correlation between these two variables with negative value [i.e., $R = -0.92$ for Daandine (S2) and $R = -0.84$ for Tipton West (S3)] indicates that more coal seam gas extraction from underground reservoirs resulted in more downward ground surface motion. For both Daandine and Tipton West, the mining operation requires groundwater withdrawal to decrease the pressure on the coal seam for extracting gas. In other words, groundwater extraction in these two fields is accompanied by underground CSG mining with strong correlation, i.e., $R = 0.63$ and $R = 0.69$ for Daandine and Tipton West correspondingly.

In the other two deformed areas showing surface deformation (i.e., Berwyndale South and Kogan North mining districts) in Fig. 8c, d, the scenario is different from that previously examined. As shown in Table 2, there is a strong correlation between CSG mining and observed deformation [i.e., $R = -0.76$ for Berwyndale South (S1) and $R = -0.86$ for Kogan North (S2)], but even with a gradual decrease in groundwater extraction during the observation period, the ground surface deformation still retained its gradual downward trend. Additionally, negative correlation between groundwater and CSG extraction (i.e., $R = -0.48$ and $R = -0.81$) in the aforementioned sites shows that the nature of CSG mining operations is not related to direct depressurization of shallow depth aquifers for both Berwyndale South and Kogan North, despite the fact that there is a report on depressurization in Berwyndale South (S1 in Fig. 5a) from 2005 for domestic groundwater extraction (QWC 2012). Taking all these observations into account, the role of compaction due to pressure depletion after water/gas pumping cannot be ruled out, and the compaction may have led to surface subsidence because of the elastic response of the sub-surface.

Conclusion

Multi-temporal space-borne SAR observations since 1992 to present day have been used to monitor the northeastern part of the Surat Basin between Miles and Dalby. Interferometric analysis for both C-band (RADARSAT-2) and L-band (ALOS PALSAR) satellite-based observations was presented between 2006 and 2014 using both stacking and

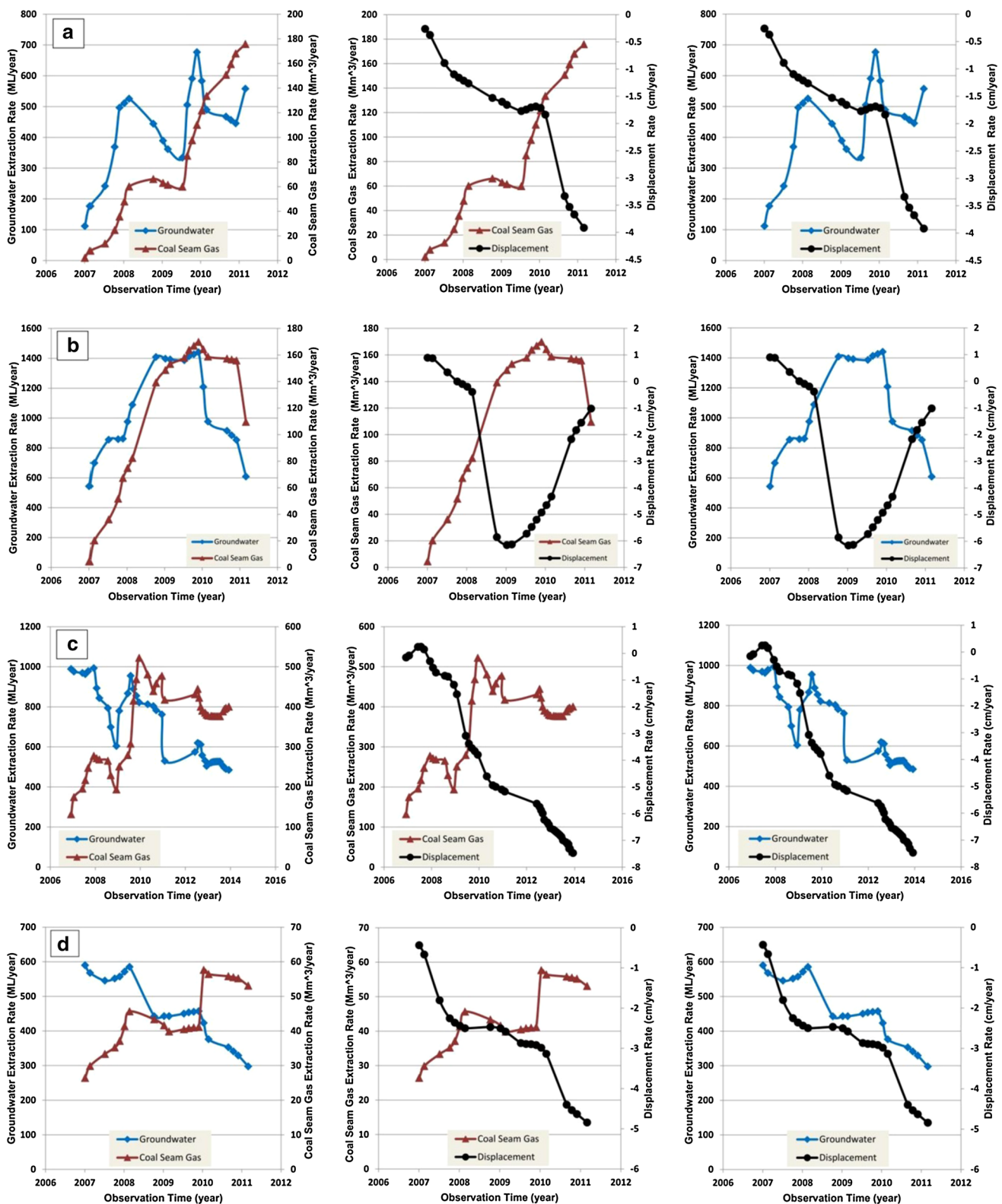


Fig. 8 Graphs of the CSG and groundwater extraction rates versus ground surface displacement in selected regions S1, S2 and S3. **a** Daandine; **b** Tipton West; **c** Berwyndale South and **d** Kogan North CSG mining districts (*yellow polygons* in Fig. 1)

SBAS processing techniques. Contrary to the previous InSAR observation (Dura et al. 2012), using different processing approach for the same dataset, ground surface deformation signals were detected in two out of four ALOS PALSAR scenes covering the area between Miles and Dalby. These signals showed a subsidence rate in excess of 2 cm/year, particularly for sites located over CSG mining with a large number of groundwater extraction wells. Comparing the space-borne long-term satellite observation to CSG extraction rates, deformation scenarios in different locations have been proposed. This observation suggests that the detected subsidence signal may have resulted from volumetric changes in the sub-surface formations and adjacent overburden due to gas extraction and associated strata compaction which can occur due to changes in pore pressure and stresses in rock matrix. As a result of associated aquifer compaction, several centimeters of land subsidence were observed using the InSAR technology. The largest values showed a rate of about 28 mm/year and are in the vicinity of Berwyndale South CSG mining area, which is correlated to large clusters of CSG extraction wells. Subsequent observation of the region with RADARSAT-2 wide frame images during 2012–2014 also confirmed the ongoing land subsidence trend in those areas. Despite implementing aquifer injection in many places around the world, including Australia, there is no record of injecting water into the shallow aquifers of this part of GAB which, incidentally, might be helpful in reversing the downward trend of groundwater supplies associated with detected spots, and in improving the balance in the volume of water withdrawal in the Surat Basin.

Last but not least, multi-temporal SAR observation not only revealed the areas with surface deformation but also facilitated the evaluation of different scenarios responsible for the detected settlement and uplift in this part of the Surat Basin. Coal seam gas mining is the prime cause for the downward motion. However, in some areas it has direct impact on shallow depth aquifer and in some others not. Considering that there is no water or gas injection initiated in the aforementioned region, the area with uplift (Fig. 6d) could be due to industrial timber forests or due to elastoplastic response of overburden layers adjacent to the CBM extraction sites.

Acknowledgments ERS and ENVISAT data were provided through a European Space Agency (ESA) Cat-1 project (P13196). ALOS PALSAR L-band acquisitions were provided through a Japan Aerospace Exploration Agency (JAXA) and Ministry of Economy, Trade and Industry METI project (P1338002). The RADARSAT-2 images were provided by the Canadian Space Agency (CSA). The authors would like to thank the Cooperative Research Center for Spatial Sciences (CRC-SI), specifically Prof. Kim Lowell and Dr. Mihai Tanase, for providing access to processing software. Finally, the support from the Geological Survey of Queensland, the Department of Natural Resource and Mines (DNRM), and Geoscience Australia

for accessing to in situ measurements and open files is gratefully acknowledged. This work was financially supported by an International Postgraduate Research Scholarship (IPRS) and Australian Postgraduate Award of Monash University, Melbourne, Australia.

References

- Amelung F et al (1999) Sensing the ups and downs of Las Vegas: InSAR reveals structural control of land subsidence and aquifer-system deformation. *J Geol* 27(6):483–486
- Anderssohn J et al (2009) Surface deformation time series and source modelling for a volcanic complex system based on satellite wide swath and image mode interferometry: the Lazufre system, central Andes. *Remote Sens Environ* 113(10):2062–2075
- Badley ME (1985) *Practical seismic interpretation*. Prentice-Hall, New Jersey
- Berardino P et al (2002) A new algorithm for surface deformation monitoring based on small baseline differential SAR interferograms. *IEEE Trans Geosci Remote Sens* 40(11):2375–2383
- Brown NJ et al (2014) Constraining surface deformation predictions resulting from coal seam gas extraction, record 2014/14. Geoscience Australia, Canberra. doi:10.11636/Record.2014.044
- Burgmann R, Rosen PA, Fielding EJ (2000) Synthetic aperture radar interferometry to measure Earth's surface topography and its deformation. *Annu Rev Earth Planet Sci* 28:169–209
- Cadman SJ, Pain L (1998) Bowen and Surat Basins, Clarence-Moreton Basin, Gunnedah Basin, and other minor onshore basins, Queensland, NSW and NT. Australian Petroleum Accumulations Report 11. Bureau of Resource Sciences, Canberra
- Casu F, Manzo M, Lanari R (2006) A quantitative assessment of the SBAS algorithm performance for surface deformation retrieval. *Remote Sens Environ* 102(3–4):195–210
- Casu F et al (2008) SBAS-DInSAR analysis of very extended areas: first results on a 60,000 km² test sites. *IEEE Geosci Remote Sens Lett* 5(3):438–442. doi:10.1109/LGRS.2008.916199
- Chaussard E et al (2013) Sinking cities in Indonesia: ALOS PALSAR detects rapid subsidence due to groundwater and gas extraction. *Remote Sens Environ* 128:150–161
- Chaussard E et al (2014) Predictability of hydraulic head changes and characterization of aquifer-system and fault properties from InSAR-derived ground deformation. *J Geophys Res Solid Earth* 119:6572–6590. doi:10.1002/2014JB011266
- Deguchi T et al (2007) Monitoring of mining induced land subsidence using L- and C-band SAR interferometry. *IEEE International Geoscience and Remote Sensing Symposium, IGARSS2007, Barcelona, Spain: 2122–21235*. doi:10.1109/IGARSS2007.4423253
- Dowson J et al (2008) Shallow intraplate earthquakes in Western Australia observed by interferometric Synthetic Aperture Radar. *J Geophys Res* 113:B11408. doi:10.1029/2008JB005807
- Dura J, Albiol D, Sabater J (2012) Baseline report on InSAR monitoring on the Surat-Bowen Basin. AL-051212_Baseline_report_01.pdf. Altamira Information
- Dzurisin D (2007) *Volcano deformation: new geodetic monitoring techniques*. Springer, Washington
- Exon NF (1976) Geology of the Surat Basin in Queensland. Bulletin 166. Bureau of Mineral Resources. Geology and Geophysics, Australia
- Featherstone WE et al (2012) Anthropogenic land subsidence in the Perth Basin: challenges for its retrospective geodetic detection. *J R Soc West Austr* 95(1):53–62
- Ferretti A, Prati C, Rocca F (2001) Permanent scatterers in SAR interferometry. *IEEE Trans Geosci Remote Sens* 39(1):8–20

- Ferretti A et al (2007) InSAR principles: guidelines for SAR interferometry processing and interpretation, TM-19. European Space Agency (ESA), The Netherlands
- Ferretti A (2014) Satellite InSAR data: reservoir monitoring from space. EAGE Publication, Houston
- Fialko Y et al (2002) Deformation on nearby faults induced by the 1999 Hector mine earthquake. *Science* 297:1858–1862
- Fielding EJ, Blom RG, Goldstein R (1998) Rapid subsidence over oil fields measured by SAR interferometry. *Geophys Res Lett* 25(17):3215–3218
- Fielding CR, Kassan J, Draper J (1996) Geology of the Bowen and Surat Basins, eastern Queensland, Australasian Sedimentologists Group Field Guide Series. Geological Society of Australia, Sydney
- Gabriel AK, Goldstein RM, Zebker HA (1989) Mapping small elevation changes over large areas: differential radar interferometry. *J Geophys Res* 94(B7):9183–9191
- Galloway DL et al (1998) Detection of aquifer system compaction and land subsidence using interferometric synthetic aperture radar, Antelope Valley, Mojave Desert, California. *Water Resour Res* 34(10):2573–2585
- Galloway DL, Hoffman J (2007) The application of satellite differential SAR interferometry-derived ground displacements in hydrogeology. *Hydrogeol J* 15(1):133–154
- Goldstein R (1995) Atmospheric limitations to repeat-track radar interferometry. *Geophys Res Lett* 22(18):2517–2520
- Green PM et al (1997) Lithostratigraphic units in the Bowen and Surat Basins, Queensland. In: Green PM (ed) *The Surat and Bowen Basins, South-East Queensland*. Queensland Minerals and Energy Review Series, Queensland Department of Mines and Energy, Queensland, pp 31–108
- Hamilton SK, Esterle JS, Golding SD (2012) Geological interpretation of gas content trends, Walloon subgroup, eastern Surat Basin, Queensland, Australia. *Int J Coal Geol* 101:21–35
- Hatherly P (2013) Overview on the application of geophysics in coal mining. *Int J Coal Geol* 114:74–84
- Hofmann-Wellenhof B, Lichtenegger H, Collins J (2001) *GPS theory and practice*. Springer, Wien
- Hooper A et al (2012) Recent advances in SAR interferometry time series analysis for measuring crustal deformation. *Tectonophysics* 514–517:1–13
- Karacan CO et al (2011) Coal mine methane: a review of capture and utilization practices with benefits to mining safety and to greenhouse gas reduction: review article. *Int J Coal Geol* 86:121–156
- Lanari R et al (2004) Satellite radar interferometry time series analysis of surface deformation for Los Angeles, California. *Geophys Res Lett* 31(L23613):1–5
- Martin MA et al (2013) Sedimentology and Stratigraphy of an intracratonic basin coal seam gas play: Walloon Subgroup of the Surat Basin, eastern Australia. *Petrol Geosci* 19:21–38
- Massonnet D, Feigl KL (1998) Radar interferometry and its application to changes in the earth's surface. *Rev Geophys* 36(4):441–500
- Moghaddam FN, Rüdiger C, Samsonov S, Walker JP, Hall M (2013) An assessment of DInSAR potential for simulating geological subsurface structure. In: Piantadosi J, Anderssen RS, Boland J (eds) *20th international congress on modelling and simulation*. Adelaide, Australia, pp 3099–3105
- Ng AH-M et al (2012) Estimating horizontal and vertical movements due to underground mining using ALOS PALSAR. *Eng Geol* 143–144:18–27
- Papendick SL et al (2011) Biogenic methane potential for Surat Basin, Queensland coal seams. *Int J Coal Geol* 88:123–134
- Petrat L, Wegmuller U (2003) Simulation of abandoned mining induced surface movements for estimating DInSAR detection limits. *IEEE International Geoscience and Remote Sensing Symposium Proceeding, IGARSS'03*
- Ramirez A, Foxall W (2014) Stochastic inversion of InSAR data to access the probability of pressure penetration into the lower caprock at In Salah. *Int J Greenhouse Gas Control* 27:42–58
- Sambridge M (1999) Geophysical inversion with a neighbourhood algorithm—I. Searching the parameter space. *Geophys J Int* 138:479–494
- Samsonov S, Van der Kooij M, Tiampo K (2011) A simultaneous inversion for deformation rates and topographic errors of DInSAR data utilizing linear least square inversion technique. *Comput Geosci* 37(8):1083–1091
- Samsonov S, D'Oreye N (2012) Multidimensional time-series analysis of ground deformation from multiple InSAR data sets applied to Virunga Volcanic Province. *Geophys J Int* 191:1095–1108
- Samsonov S, D'Oreye N, Smets B (2013) Ground deformation associated with post-mining activity at the French-German border revealed by novel InSAR time series method. *Int J Appl Earth Obs Geoinf* 23:142–154
- Samsonov S et al (2014) Rapidly accelerating subsidence in the greater Vancouver region from two decades of ERS-ENVISAT-RADARSAT-2 DInSAR measurements. *Remote Sens Environ* 143:180–191
- Sandwell DT, Price EJ (1998) Phase gradient approach to stacking interferograms. *J Geophys Res Solid Earth* 103(B12):30183–30204
- Sansosti E (2010) Space-borne radar interferometry techniques for generation of deformation time series: an advanced tool for Earth's surface displacement analysis. *Geophys Res Lett* 37(20):L20305
- Scott SG (2008) The geology stratigraphy and coal seam gas characteristics of the Walloon subgroup-northeastern Surat Basin. Dissertation, James Cook University
- Tarayre H, Massonnet D (1996) Atmospheric propagation heterogeneities revealed by ERS-1. *Geophys Res Lett* 23:989–992
- Tan PL et al (2010) Tools for water planning: lessons, gaps and adoption. *Waterlines report, Part. 3*. National Water Commission. Canberra
- Vasco DW, Rucci A, Ferretti A, Novali F, Bissell RC, Ringrose PS, Mathieson AS, Wright IW (2010) Satellite-based measurements of surface deformation reveal fluid flow associated with the geological storage of carbon dioxide. *Geophys Res Lett* 37(3):L03303. doi:10.1029/2009GL041544
- Veil JA et al (2004) A white paper describing produced water from production of crude oil, natural gas, and coal bed methane. US Department of Energy. National Energy Technology Laboratory, Under Contract W-31-109-Eng-38
- Williams S, Bock Y, Fang P (1998) Integrated satellite interferometry: tropospheric noise, GPS estimates and complications for interferometric synthetic aperture radar products. *J Geophys Res B Solid Earth* 103(B11):27051–27067
- Zahiri H (2012) Integration of synthetic aperture radar interferometry (InSAR) and geographical information systems (GIS) for monitoring mining induced surface deformations. Dissertation, Curtin University
- Zebker HA, Villasenor J (1992) Decorrelation in interferometric radar echoes. *IEEE Trans Geosci Remote Sens* 30(5):950–959
- Zebker HA, Rosen PA, Hensley S (1997) Atmospheric effects in interferometric synthetic aperture radar surface deformation and topographic maps. *J Geophys Res B Solid Earth* 102(B4):7547–7563
- Zhu W et al (2014) Landslide monitoring by combining of CR-InSAR and GPS techniques. *Adv Space Res* 53(3):430–439

Web references

- APLNG (2010) Environmental impact statement—Volume 5, Attachment 21: groundwater technical report—Gas Fields. http://www.aplng.com.au/pdf/eis/Volume_5/Vol5_Att_21-GroundWater_Gasfields.pdf. Accessed 12 Oct 2013
- CSIRO (2012), Coal seam gas-produced water and site management (fact sheet). <http://www.csiro.au/news/coal-seam-gas#FactSheets>. Accessed 5 Oct 2013
- DNRM (2012). <https://www.mines.industry.qld.gov.au>. Accessed 2013
- Queensland Water Commission (QWC) (2012) Underground water impact report for the Surat Cumulative Management Area (CMA), Coal Seam Gas Water, State of Queensland. <https://www.dnrm.qld.gov.au/ogia/surat-underground-water-impactreport>. Accessed 20 Oct 2013
- Queensland Gas Company (QGC) (2013) Report for QWC-17-10 (Stage 3 WMMP): CSG water monitoring and management plan. http://www.qgc.com.au/ebooks/QGC_Stage_3_WMMP_Dec_13/index.html#/1/. Accessed 21 Mar 2014
- Simons M, Rosen PA (2007) Interferometric synthetic aperture radar geodesy. *Treatise on Geophysics, Geodesy*, 3, 391-446. <http://resolver.caltech.edu/CaltechAUTHORS:20130612-140139779>. Accessed 15 Sept 2014
- Statistics Canada (2009) Seasonal adjustment and trend-cycle estimation, Statistics Canada Quality Guideline, 5th edition, Catalogue no. 12-539-X. <http://www.statcan.gc.ca/pub/12-539-x/2009001/seasonal-saisonnal-eng.htm>. Accessed 16 Jan 2015